Influence of Nozzle geometry on spray shape, particle size, spray velocity and Air entrainment of high pressure Diesel spray

Camille Hespel, Jean-Bernard Blaisot, Xandra Margot, S. Patouna, Armelle Cessou, Bertrand Lecordier

Influence of Nozzle Geometry on Spray Shape, Particle Size, Spray Velocity and Air Entrainment **of High Pressure Diesel Spray**

C. Hespel[1-2], J.B. Blaisot[1], X Margot[3], S. Patouna[3],A. Cessou[1], B. Lecordier[1]

[1]CORIA – UMR 6614, CNRS, Université et INSA de Rouen
E-mail: Jean-Bernard.Blaisot@coria.fr
Telephone: +33 (0) 2 32 95 36 76
Fax: +33 (0) 2 32 91 04 85

[2] INSTITUT PRISME, Université d'Orléans, 8 rue Léonard de Vinci 45072 – Orléans, FRANCE
E-mail: camille.hespel@univ-orleans.fr
Telephone: +33 (0)2 38 49 31 46
Fax: +33 (0)2 38 41 73 83

[3]CMT–Motores Térmicos. Universidad Politécnica de Valencia. Camino de Vera s/n, 46022 Valencia, SPAIN
E-mail: xmargot@mot.upv.es
Telephone: +34 963 877 650
Fax: +34 963 877 659

Abstract. Air/fuel mixing process in the combustion chamber of Diesel engines plays an important role on the combustion efficiency. This mixing depends on the particle size distribution in the spray, on the local velocity of fuel droplets in the spray and on the air entrainment. Nozzle geometry as well as nozzle internal flow conditions influence many of these spray properties. An experimental study of the influence of the nozzle geometry on these properties has been conducted. The spray structure and the particle size distribution are determined using image shadowgraphy, the axial velocities near the nozzle outlet have been measured using Laser Correlation Velocimetry. Gas velocities are measured using Fluorescent Particle Image Velocimetry. It is found that the cavitation plays a role of major importance on the atomization process and on the interaction between the liquid spray and the surrounding gas.

Notation

C_a	*orifice area-contraction coefficient*
C_d	*orifice Discharge Coefficient*
C_v	*orifice velocity Coefficient*
d	*orifice diameter*
D_{30}	*arithmetic mean diameter*
D_{32}	*Sauter mean diameter of droplets*
D_{43}	*arithmetic mean diameter of volume-based drop-size distribution*
Ke	*entrainment coefficient*
$\dot{m}_a$	*mass flow rate x=a (air) x=f (fuel)*
P_{inj}	*Injection pressure*
P_c	*Discharge pressure*
X	*radial coordinate of the spray*
Z	*axial coordinate of the spray*
Θ	*Spray cone angle*
ρ_x	*density*

Introduction

Injection is one of the key parameters in engine control. Indeed, combustion processes in Diesel engines greatly depend on the characteristics of the injection. Atomization and mixing are the first two processes of a long and complex chain which ends in the formation of pollutants. Thus, in the context of pollutant emission reduction, advanced knowledge of injection features is still needed. It is well-known that the atomization of the jet strongly depends on the nozzle geometry. The shape of the nozzle affects the cavitation phenomenon in the nozzle and therefore the spray characteristics. To visualise the internal flow and the structure of cavitation in multi-holes and real-size nozzles is not obvious. This has been done on large-scale transparent nozzles by Soteriou et al (1998) or on single-hole real-size nozzle by Badock et al (1999). Here the internal flow is investigated through numerical simulations while the jet emanating from the nozzle exit is characterized experimentally.
This work is a part of a program which aims at improving our capacity to predict in a fine way all the processes of atomization. Numerical simulations of the flow in the nozzle as well as experiments on the spray emanating from the nozzle have been done to characterize the injection process. Complementary results obtained through experiments and CFD simulations give a better understanding of the injection.
The effect of the nozzle geometry on the atomization processes is straightforward. This study is focused on the comparison of two nozzle geometries. Two 6-hole nozzles are used, one with cylinder-shaped holes (Kf0) and the other with cone-shaped holes (Ks1.5). The main difference between these two nozzles concerns the cavitation that is expected to occur more frequently for Kf0 nozzle.
Experimental conditions and measurement techniques used in this work are presented in the next section. A comparison of the results for the two nozzle geometries follows, based on spray features measured during the stationary phase of injection. The particular behavior of the injectors during transient phases is then presented for experiments done in multi-injection conditions. A conclusion ends this paper.

Methodology

For the analysis presented in this work, an experimental set-up described below was used that included the injection system and the optical techniques for the measurement of the macro- and micro-scale characteristics of the spray. In addition, some CFD calculations of the internal nozzle flow were performed to help explain the behavior of the sprays, which is known to be influenced by the presence of cavitation.

Injection system and test bomb

Injection Nozzles

Two different six holes Common Rail Diesel solenoid injectors working under injection pressure of up to 1500 bar have been considered in this investigation, one with cylinder-shaped holes (type Kf0) with an orifice diameter of 147 µm, the other with cone-shaped holes of type Ks1.5 with nozzle exit diameter of 138 µm. The geometry of the holes has been measured with a particular technique described in (Macián et al., 2003), whereby a special type of silicone is used to obtain an internal mould of the nozzles (

Fig. **1**). Photographs of the moulds are taken with a microscope, and then loaded on a computer aided design (CAD) software with the appropriate scale factor. The dimensional characterization of the nozzle can thus be obtained. This experimental technique is useful for the study of the Diesel nozzle internal flow, as it allows establishing relationships between the internal geometry, the flow characteristics and the subsequent spray behavior.

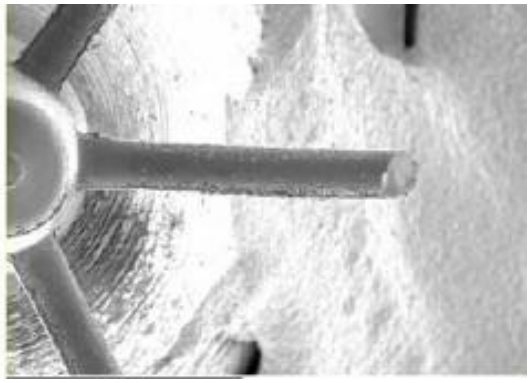

Fig. 1. Silicone mould of injector

Fig. 2. Nozzle with deflector

The nozzle geometries and operation conditions have been chosen in order to obtain different cavitation levels. The cylindrical holes promote the cavitation, while the cone-shaped holes limit significantly this phenomenon.

Only one of the six jets is investigated in each case. In order to avoid the interaction between jets, a small deflector that does not change the behavior of the injector is placed over the nozzle (Fig. 2).

Measurement conditions

The experiments were performed in a high pressure bomb with different optical accesses. The operating conditions are summarized in table 1. The test oil was dodecane, a non-fluorescent fuel with physical properties similar to those of the Diesel fuel (ρ_f=750 kg/m3). The reference time was given by the start of activation (SOA) of the main injection. Therefore, for the double injection the beginning of pilot injection was -416.16 µs or -832.3 µs for 5°CA and 10°CA respectively. The hydraulic delay was 306 µs for the Kf0 nozzle and 340 µs for the Ks1.5 nozzle for a back-pressure of 1 MPa. The difference between hydraulic delays disappeared for a back-pressure of 5 MPa

Table 1. Experimental test conditions

Parameters	Values
Discharge pressure Pc	1 MPa, 5 MPa
Injection pressure Pinj	80 MPa, 150 MPa
Single injection duration	500 µs, 1000µs
Double injection duration	200 µs (pilot), 500 µs (main)
Dwell angle (double injection)	5°CA, 10°CA @ 2000 rpm

Internal nozzle flow CFD approach

Some calculations were computed with the commercial CFD code STAR-CD, v 4.06 for the different measurement conditions, with the objective of better understanding the influence of the inner flow characteristics on the spray evolution.

Considering the 60^o periodic symmetry of the six-hole injector, the computational domain meshed was a 60^o sector, based on the exact geometry of one of the six nozzles chosen as being representative of all. The calculations were performed for the full lift configuration (250 µm). Symmetry boundaries were defined to model the geometric periodicity, and constant pressure was prescribed at both the inlet and outlet boundaries. A grid independence study allowed determining the mesh fineness, which resulted in a total of about 600.000 cells, with a cell size of 10 µm approximately.

All calculations presented here were performed using the conventional k-ε turbulence model with hybrid near wall treatment. The cavitation model implemented in this code is based on the Rayleigh equation [Rayleigh 1917], which links the rate of change of the bubble radius with the local pressure. In this model both the liquid and vapor densities are constant and there is no slip between bubbles and liquid. Details of the complete numerical approach set-up are given in Margot et al. 2010.

It should be noted that the working liquid was Diesel fuel with the corresponding properties.

Imagery

Large field

The experimental setup for shadowgraphy consists of a CCD-camera with a lens of 50 mm focal length illuminated by a pulsed source in an on-axis configuration. A light panel connected to a stroboscope provides a uniform background illumination.

The field of view is 69x53mm² with a resolution of 11pix/mm. At least 30 pictures per operating point were analyzed to provide the mean penetration length and cone angle of the spray. Penetration length up to 80 mm was measurable thanks to the inclined position of the jet in the field of view.

Small field

Granulometry measurements were performed by imagery. The setup includes the same camera, a long working distance microscope and nanolite source (flash duration about 11ns) (2005; Fdida and Blaisot 2010).

).

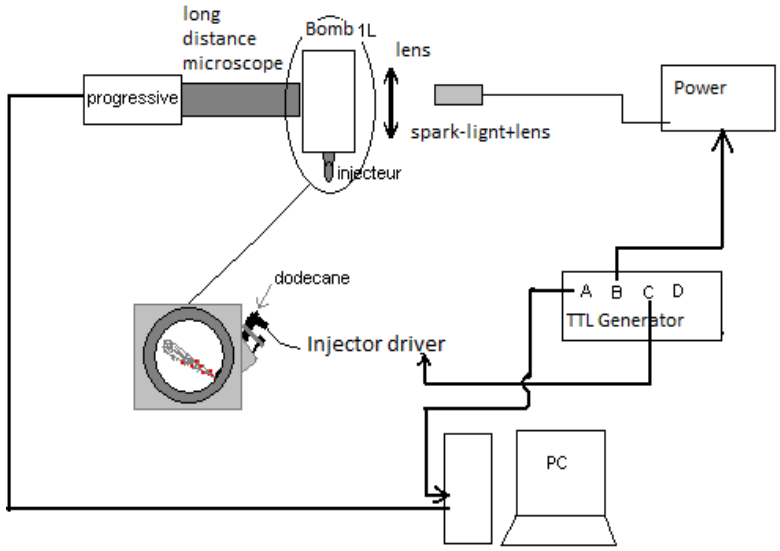

Fig. 3 Experimental setup of the granulometry by imagery

A lens arrangement provides a uniform illumination over the field of view which is 650x496 µm² (resolution =1170 pix/mm). A specific image processing analyzes the gray levels images in order to determine the diameter and the shape of droplets in a control volume limited by the field of view and depth from focus (Blaisot and Yon 2005; Fdida and Blaisot 2010).

Long distance laser correlation velocimeter

This technique is an application to dense liquid sprays of the time-of-flight measurement principle (Chaves et al 1993). The one-beam two images configuration (Schugger and Renz 2002) has been adapted for the measurement in the pressure chamber with the replacement of the single imaging lens by a long working distance microscope. The setup is composed of one laser beam (HeNe) illuminating the spray and an optical system imaging the two measurement points on photomultipliers coupled to optical fibres. The long distance microscope can image the spray at a reasonable distance between the imagery system and the image plane with the needed magnification. The magnification factor is 40 for a distance between the objective and image plane of 930mm (Fig. 4). The interval between the fibres is 940 µm, giving an interval of 50 µm between the measurement volumes. Since any structure passing in the first measurement volume has a high probability of passing also in the second one, the first signal precedes the second one by a minor delay.

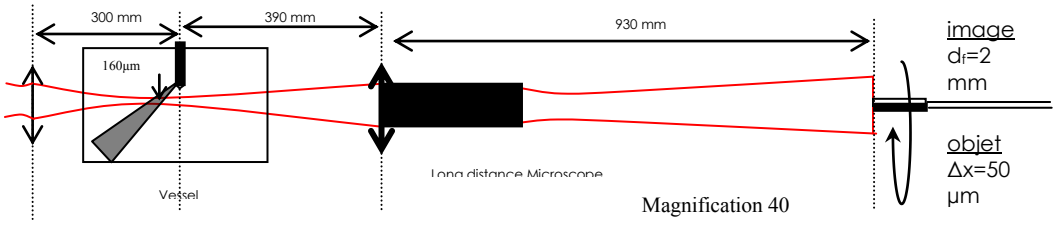

Fig. 4: Experimental apparatus of the laser correlation long distance velocimeter

This time delay is used to calculate the spray velocity. The time delay between the two signals, due to the time-of-flight, is calculated using a cross correlation algorithm between the signals on sliding time windows. A detailed description of the evaluation and validation method can be found in (Kirmse et al 2004), an error-analysis is carried out in (Kirmse et al 2002).

Fluorescent-Particle Image Velocimetry

Velocity fields are measured using the Particle Imaging Velocimetry (PIV) technique based on fluorescent droplets for the liquid phase or on fluorescent seeds for the ambient gas (Fig. 5). Due to the different dynamic velocities between air and fuel in Diesel jets, the ambient gas and fuel droplets velocity fields are not measured simultaneously. Fluorescence images were preferred to Mie scattering images because liquid and vapour phases can be discriminated and the multi-scattering effect is reduced. The gas phase is seeded with small droplets tagged with pyrromethene 597 (2g/L). This dye offers a relatively narrow emission spectrum around 590 nm for 532 Yag excitation (Wolff et all 2007). The fluorescence signal is detected by an intensified CCD camera (Hamamatsu) through high pass filter (OG550). The Mie scattering of laser light is strongly reduced by this filter. The time delay between the two laser pulses is chosen between 50 µs and 200 µs for measurement on the gas phase, and standard PIV algorithms are used to obtain the ambient gas velocity field. A typical mean ambient gas velocity field is shown in Fig. 5b. The liquid phase velocity is determined by seeding the fuel with the same fluorescent dye species (5mg/L of pyrromethene are fully soluble in dodecane). The addition of this dye does not affect the injector behavior. Liquid phase velocity fields are measured with a time difference between the two exposures of 5 µs. The fuel droplets are well localized in the images because the specific spectral filter avoids the problem of Mie multi-scattering. An in-house post-processing is applied on images to extract each particle and the velocity field is determined on an irregular mesh centred on each particle. The PIV algorithm used to determine velocity fields for the liquid phase was developed in the laboratory (Kosiwckuk et al 2005). An example of the mean velocity field is shown in Fig. 5c.

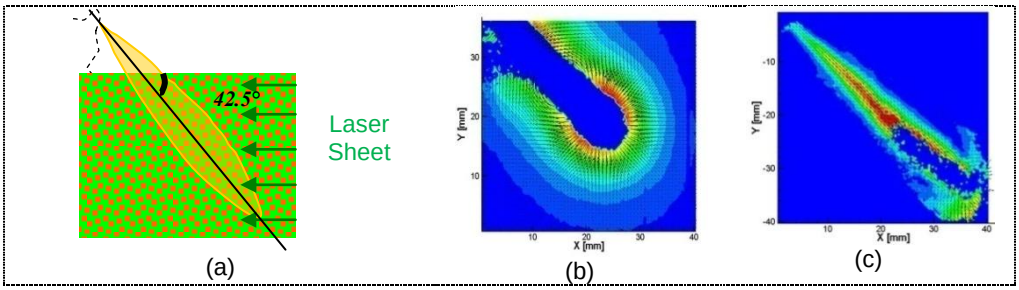

Fig. 5 : Fluorescent particle image velocimetry: geometrical configuration (a), mean velocity for the gas phase (b) and mean velocity field for the liquid phase (c)

Comparison of nozzle geometries for the stationary phase

The influence of the nozzle geometry on the spray characteristics is investigated for the quasi-steady phase of injection for activation duration of 1000 µs.

Spray cone angle

The cone angle is defined as the angle between both edges of the spray on the first third of the penetration length. The variation of the cone angle versus time is presented in Fig. 6. As expected, the cone angle increases significantly with back-pressure P_c and it is larger for the cylindrical nozzle Kf0. This figure also shows that the difference between the cone angles of the Kf0 and Ks1.5 nozzles reduces when P_c increases. Indeed, the mean cone angle (determined along the stationary phase of injection) for the Kf0 nozzle is 15.3°, while it is 12.6° for the Ks1.5 for P_c=1 MPa (with a standard deviation of 0.7). So the difference in cone angles is 2,7^o for P_c=1 MPa, whereas it is only around 1° for Pc = 5 MPa.

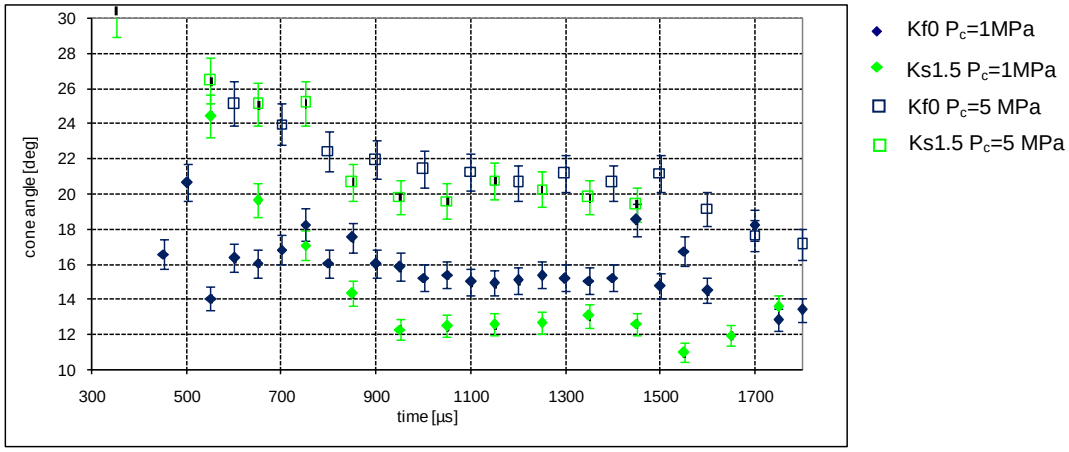

Fig. 6 : Development of spray cone angles, measured at 80 MPa of injection pressure

The computations performed for this case allow explaining these results, as illustrated in Fig. 7, which shows the images of the volume fraction of vapour in both nozzles for the two different back pressures. Indeed, for an injection pressure of 80 MPa, large cavitation zones develop along the cylindrical nozzle for both P_c=1 MPa and P_c=5 MPa. In the case of 1 MPa back-pressure, however, the cavitation bubbles reach the nozzle exit, while at higher back-pressure, they clearly do not. In the conical nozzle, there is no cavitation for any of these operation conditions. This observation highlights that when cavitation reaches the hole exit, the spray cone angle becomes wider for a given back-pressure. When there is no cavitation at the nozzle exit, however, the spray cone angle is assumed to be mainly related to the gas density. At 5 MPa back-pressure, the density of the flow is similar at the exit of both nozzles, hence, the spray cone angles are also very similar.

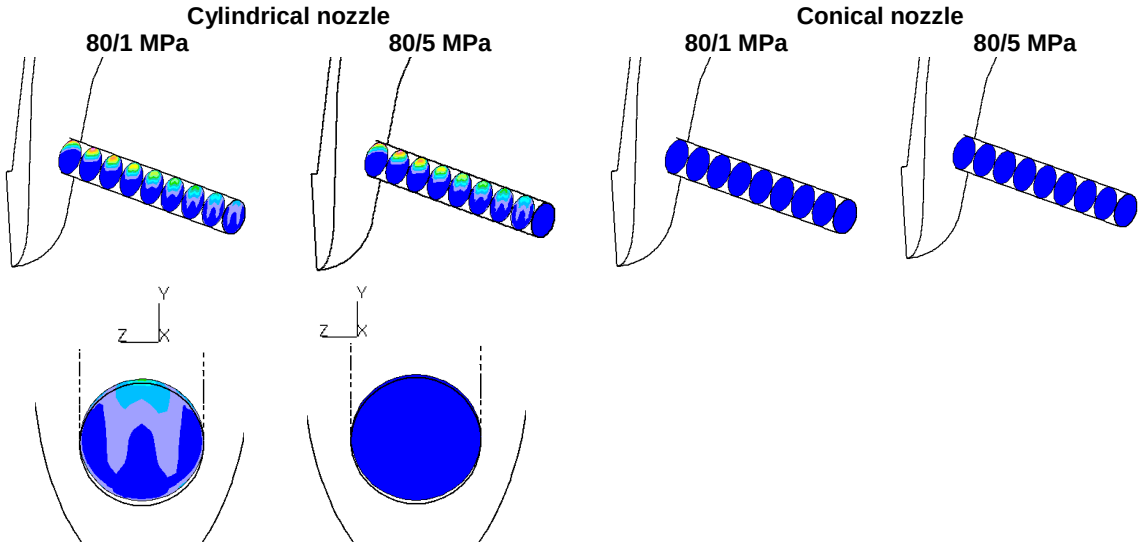

Fig. 7 : Cavitation pattern for the cylindrical and conical nozzle at 80/1 and 80/5 MPa. Color scale: 0-1

Liquid phase velocity

The velocities in the liquid phase close to the nozzle exit were measured using the long distance Laser Correlation Velocimeter (LCV). For the case of 80 MPa injection pressure and 1 MPa back-pressure, radial profiles of the axial velocity normalized by the frictionless velocity are shown in Fig. 8 for two positions: 10 mm (a) and 25 mm (b) downstream of the nozzle exit. The geometry of the nozzle does not seem to affect the normalized profiles, which are very similar for both the Kf0 and the Ks1.5 holes. The maximum velocity in the centre of the jet reaches about 35% of the frictionless velocity.

The mass flow rate measured using an EFS EMI2 mass flow meter is higher for the Ks1.5 nozzle, although its orifice exit diameter is smaller than the cylindrical one. Indeed, it has a higher discharge coefficient of 0.88, against 0.74 for the Kf0 nozzle.

The discharge coefficient is defined as the product between the area-contraction coefficient C_a and the velocity coefficient C_v. Since the velocity profiles for both geometries are similar, it seems reasonable to assume that the velocity coefficients are very close for the two nozzles. Hence, the area-contraction coefficient C_a, which is an indicator of the effective flow area section compared to the orifice section, is smaller for the cylindrical nozzle, due to the presence of the cavitation bubbles at the exit. Indeed, it is known that the effective area can be reduced because of vapor bubbles reaching the orifice exit (Chaves et al 1995).

LCV measurements did not indicate that there is an effective section reduction, probably due to the fact that velocity is measured on every fluid structure passing through the LCV probe, whatever its nature, i.e. a droplet, a ligament or a cavitation bubble.

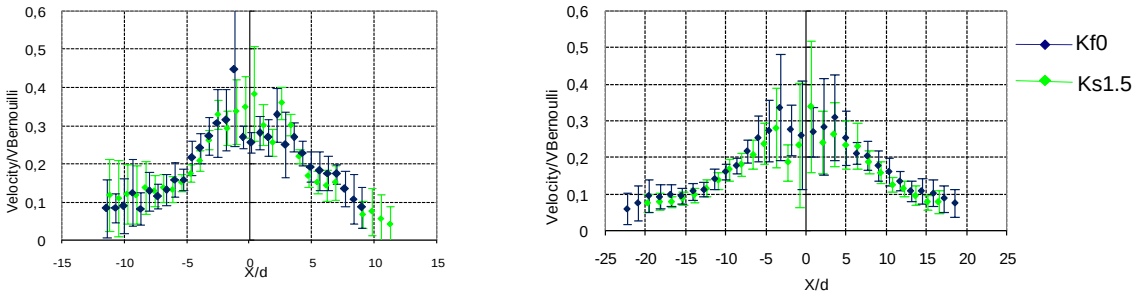

a) 10 mm downstream of the nozzle b) 25 mm downstream of the nozzle

Fig. 8 Radial profiles of the axial spray of the velocities Kf0 and Ks1.5 nozzle, P_c=1MPa, P_{inj}=80Mpa.

Drop size distribution

The size of the droplets is estimated using the image processing of over 100 pictures for each point. The mean diameters measured 10 mm downstream of the nozzle exit and at 2 mm from the jet axis are reported in Table 2. As expected, the injection pressure has a significant influence on the reduction of the droplets size in the spray, whatever the nozzle.

Table 2. Mean diameters of droplet size distributions

	Kf0		Ks1.5	
P_{inj}=80 MPa P_c=	**1 MPa**	**5 MPa**	**1 MPa**	**5 MPa**
D30 [µm]	7.4	9.1	9	8.5
D32 [µm]	8.4	10.6	10.2	10.3
D43 [µm]	9.6	12.2	11.4	11.9
P_c=1 MPa P_{inj}=	**80 MPa**	**150 MPa**	**80 MPa**	**150 MPa**
D30 [µm]	7.4	6.3	9	7.2
D32 [µm]	8.4	7.1	10.2	8
D43 [µm]	9.6	7.9	11.4	8.9

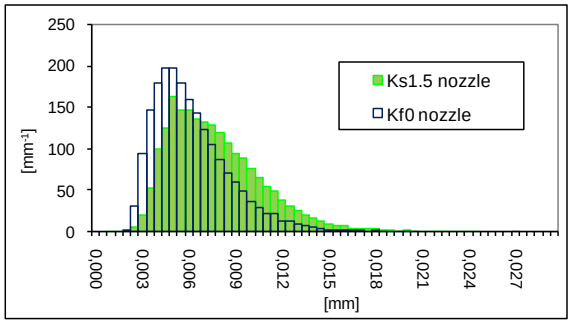

Fig. 9 Droplets size distribution for P_{inj}=80 MPa and P_c=1 MPa

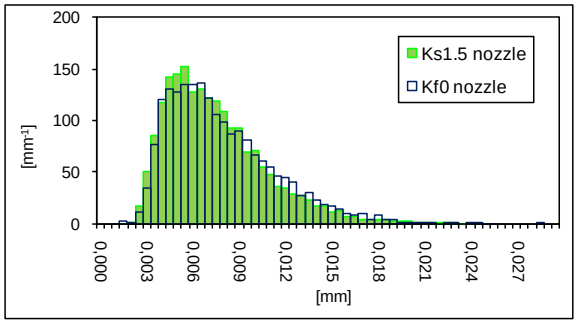

Fig. 10 Droplets size distribution for P_{inj}=80 MPa and P_c=5 MPa

Rising the ambient pressure from 1 MPa to 5 MPa has also an effect on the drop size distribution, though only for the Kf0 nozzle, as illustrated in Fig. 9 and Fig. 10. Indeed, the droplets size distributions for the Ks1.5 nozzle are very similar for both back-pressures, and Fig. 10 shows that for 5 MPa back-pressure, the size distribution of the cylindrical nozzle is also very similar to that of the conical nozzle. However, for the cavitating case, Kf0 and 1 MPa back-pressure, it differs significantly from the others: the cavitation results in a production of larger droplets close to the nozzle exit, and smaller droplets further downstream.

Gaseous Phase velocity and air entrainment

Mean gas velocity fields taken around 750 µs after SOA are presented in **Erreur ! Source du renvoi introuvable.**, which shows the development of a vortex in the air. The centre of this vortex follows the variation of the penetration length and remains located around 80% of spray length over the injection duration. Low velocities (<2m/s) are measured in the gas, as also found in other studies (Le Moyne et al 2007). The slow motion of the gaseous phase comes from a low momentum exchange between liquid and gas.

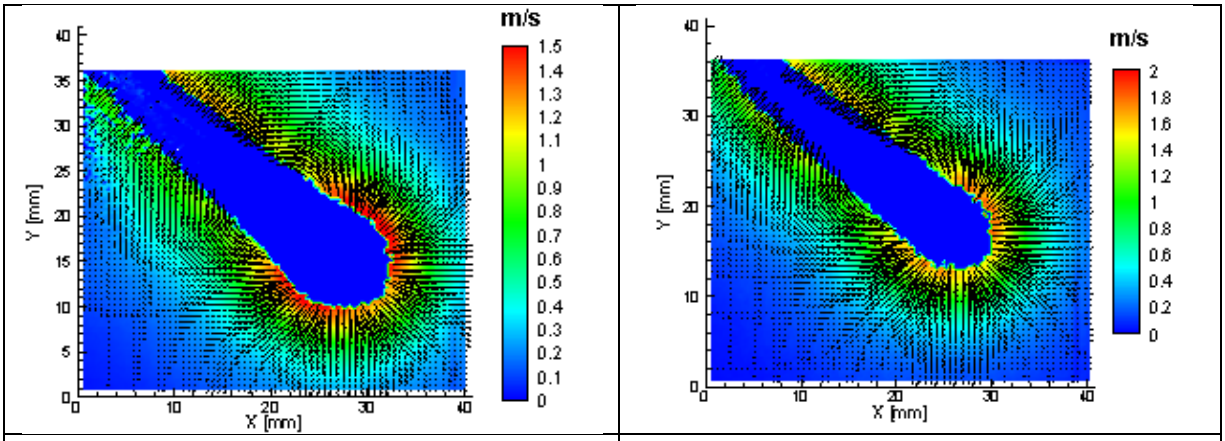

a) Ks1.5: 750-850µs after SOA

b) Kf0: 650-750µs after SOA

Fig. 11 Mean air velocity fields for P_{inj}=80 MPa and P_c=1 MPa

The air entrainment has been calculated on the average velocity fields following the method of Cossali et al (1991). A reference surface limited by a cylinder of radius R around the spray is defined for each field. The air mass flow rate $\dot{m}_a$ cumulated through this reference surface is determined by equation 1. The local air flow rate $\frac{d\dot{m}_a}{dz}$ is shown in **Erreur ! Source du renvoi introuvable.**a for P_{inj} = 80 MPa and P_c = 1 MPa. It takes a positive value near the nozzle, where the air motion is oriented towards the spray and negative where the air is moving away from the spray at the spray tip. The zero crossing is located at the centre of the vortex. The same maximum flow rate of 0.6 g/s is reached for

the two nozzles. For two-phase flows, Cossali et al (1991) proposed to estimate the mixing performance of nozzles by the entrainment coefficient *Ke* given by equation 2.

$$\dot{m}_a(z) = \rho_a \, 2\pi \, R \int_0^z U_r(\xi) d\xi \qquad \text{Eq. 1}$$

$$Ke = \frac{d\dot{m}_a}{dz} \frac{\mathrm{d}}{\dot{m}_f} \sqrt{\frac{\rho_f}{\rho_a}} \qquad \text{Eq. 2}$$

This coefficient is greater for the Kf0 nozzle (see **Erreur ! Source du renvoi introuvable.**b) because the orifice diameter is greater and the fuel flow rate is smaller for this nozzle.

The mixing rate, defined as the ratio between cumulated air mass flow rate and fuel mass flow rate, is shown in **Erreur ! Source du renvoi introuvable.**c. The maximum mixing rate is located at the vortex centre location. As the velocity field measurements begin 8 mm downstream of the nozzle exit, the mixing rate is underestimated.

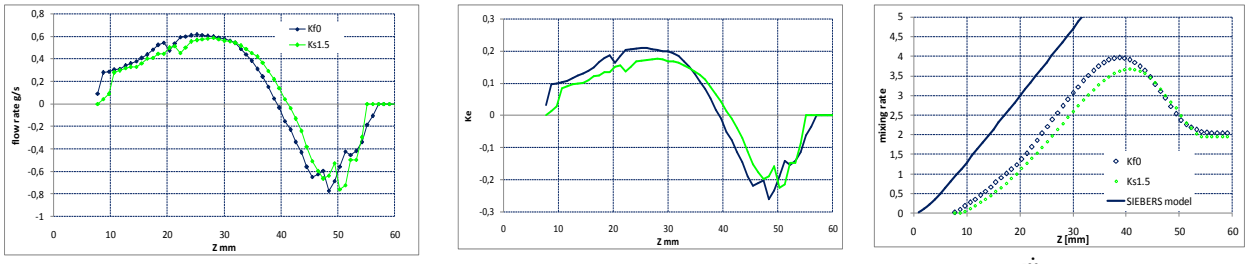

a) Flow rate b) entrainment coefficient c) mixing rate $\frac{\dot{m}_a}{\dot{m}_f}$

Fig. 12 Air entrainment performances of nozzles for P_c = 1 MPa and P_{inj} = 80 MPa, 950 µs after SOA

However, the slope is very similar to that predicted by Siebers model (Siebers 1999) expressed by equations 3 and 4. It is worth noting that the wider cone-angle of the Kf0 nozzle improves the performance of this nozzle in terms of momentum transfer from droplets to ambient air.

$$\frac{\dot{m}_a}{\dot{m}_f} = \frac{1}{2}\left(\sqrt{1 + 16\,\tilde{Z}^2} - 1\right) \qquad \text{Eq. 3}$$

$$\tilde{Z} = \frac{z}{\sqrt{\frac{\rho_f}{\rho_a}} \frac{\mathrm{d}\sqrt{c_a}}{a.\tan\left(\theta/2\right)}} \quad \text{with } a\text{=0,66} \qquad \text{Eq. 4}$$

Behavior of injector during transient phases for multi-injection condition

Penetration length

Penetration lengths obtained for a single injection (500 µs) or a pilot (200 µs) and a main injection (500 µs) are reported in Fig. 13 for two injection pressures: 80 MPa and 150 MPa. The influence of the pilot injection on the main injection is more significant for P_{inj} = 80 MPa. In the case of a pilot injection occurring 5°CA before the main injection, the lapse of time between closing and opening is 216 µs only, which is too short to obtain a complete closing of the needle at the end of the pilot injection. When the delay between the pilot and main injections is greater than 10°CA, the effect of the first injection disappears. In this case, the time between the two injections is long enough to obtain a complete closing of the needle before the second activation. For high injection pressure (150 MPa), the closing and opening times are shorter and there is sufficient time for the needle to close before the

second injection, whatever the delay. In this case, the evolution of the penetration length versus time is very similar for all injections.

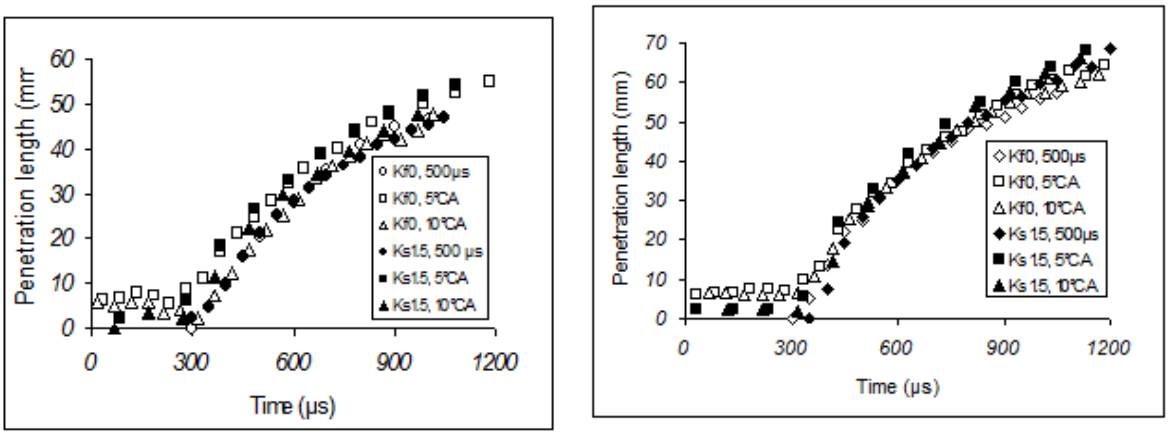

a) P_{inj} = 80 MPa, P_c = 1 MPa b) P_{inj} = 150 MPa, P_c = 1 MPa

Fig. 13 : Penetration length versus time

Liquid phase velocity

The velocity measured by VLC shows that the main jet is faster at the beginning of the main injection when there is a pilot injection than when there is a single injection. This effect persists for the Kf0 nozzle up to Z = 25 mm although it disappears at this distance for the Ks1.5 nozzle (see Fig. 14). The longer penetration lengths obtained for the double injection confirm this.

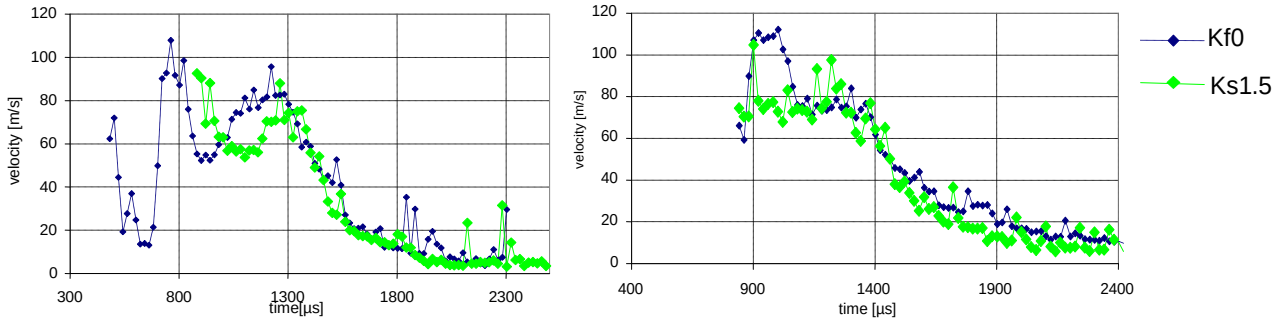

a) P_{inj}=80 MPa, P_c=1 MPa, Z=10 mm, X=-0.78 mm b) P_{inj}=80 MPa, P_c=1 MPa, Z=25 mm, X=-1.2 mm

Fig. 14 velocity versus time for the 200+500µs 5°AC

Gaseous phase velocity and air entrainment

The effect of the pilot injection on air entrainment is reported for the Kf0 nozzle only, at P_{inj}=80 MPa and P_c=1 MPa. The effect of a pilot injection 5°CA before the main injection on the entrainment coefficient is mainly related to the longer penetration length, whatever the delay after the main injection activation. This is illustrated in Fig. 15 (a) and (b). As the penetration length is greater with a pilot injection 5°CA before the main injection, the zone of induced gas flow oriented toward the spray axis is also longer. The maximum mixing rate is thus greater with a pilot injection 5 °CA before main, just because the spray is longer in this case. However, since the mixing rate slopes are the same for the three types of injection, it seems that the pilot injection does not improve the momentum exchange induced by the spray (Fig. 15c).

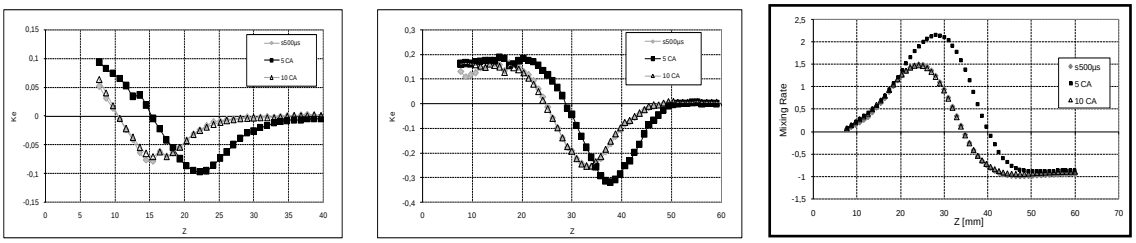

a) Entrainment coefficient t=450 µs b) Entrainment coefficient t=650µs c) Mixing rate t=650 µs

Fig. 15. Kf0 nozzle, P_{inj}=80 MPa P_c=1 MPa

Conclusions

The investigations presented here for different nozzle geometries (cylindrical and conical) demonstrate that the cavitation plays a major role on the atomization process and on the interaction between the liquid spray and the surrounding gas. Calculations have shown that the cavitation bubbles may reach the cylindrical nozzle exit, especially when the back-pressure is relatively low.
When the levels of cavitation are low and do not reach the nozzle exit, measurements show that the two nozzles behave similarly. For example, at moderate injection pressure and high back pressure, the spray cone angles as well as the drop size distributions of the two tested nozzles are very similar. Differences occur when cavitation is generated in the cylindrical nozzle. The measurements have shown that the cavitation favours a wider spray angle and so improves the air entrainment, and promotes the production of smaller droplets. However, the cavitation does not seem to influence the spray velocities: indeed, the velocity profiles and the penetration lengths are similar for the two nozzles. These are more sensitive to the needle dynamics.

Acknowledgments

Part of this work has been performed in the framework of the PREDIT program "EMPhASE", supported by the French Environment and Energy Management Agency (ADEME).

References

Blaisot J.B. and Yon J. (2005) Droplet size and morphology characterization for dense sprays by image processing: application to the Diesel spray, Exp. Fluids 39, 977–94

Badock C., Wirth R. Fath A., Leipertz A.(1999) Investigation of cavitation in real size diesel injection nozzles, International Journal of Heat and Fluid Flow 20 pp538-544

Chaves H., Knapp M., Kubitzek A., and Obermeier F. (1993) High speed flow measurement within an injection nozzle, SPIE, vol. 2052, Laser Anemometry Adv. and Applications

Chaves H., Knapp M., and Kubitzek A. (1995) Experimental study of cavitation in the nozzle hole of Diesel injectors using transparent nozzles, SAE - 950290

Cossali G.E., Brunello G., Coghe A. (1991) LDV Characterization of air entrainment in transient diesel spray, SAE - 910178

Fdida N. and Blaisot J.B. (2010) Drop size distribution measured by imaging: determination of the measurement volume by the calibration of the point spread function, Meas. Sci. Technol. 21 025501 (15pp)

Kirmse C., Chaves H. and Obermeier F. (2002) Korrelationsvelocimetrische Untersuchungen des Diesel-Einspritzstrahls einer Common-Rail Einspritzung, Proc. SPRAY, pp285-293

Kirmse C., Chaves H. and Obermeier F. (2004) Velocity measurements of dense Diesel fuel sprays in dense air, Atomization and Sprays, vol 14 pp589-609

Kosiwckuk W., Cessou A., Trinité M., and Lecordier B. (2005) Simultaneous velocity field measurements in two-phase flows for turbulent mixing of spray by means of two-phase PIV, Experiments in Fluids, 39, p.895-908

Lemoyne L., Guibert P., Roy R., and Jeanne B. (2007) Fluorescent-PIV spray/air interaction analysis of high-pressure gasoline injector, SAE- 2007-01-1825, JSAE 20077121 pp109-118

Macián V., Bermúdez V., Payri R., and Gimeno J. (2003) New technique for the determination of the internal geometry of Diesel nozzle with the use of silicone methodology, Experimental Techniques 27 (2), pp39-43

Margot X., García A., Fajardo P., and Patouna S. (2010) Analysis of the cavitating flow in real size diesel injectors with fixed and moving needle lift simulations. Proceedings of the Fifth European Conference on Computational Fluid Dynamics, ECCOMAS CFD 2010.

Rayleigh L (1917) On the pressure developed in a liquid during the collapse of a spherical cavity. Phil. Mag. vol 34: pp 94-98.

Schugger C. and Renz U. (2002) Influence of spray velocity and structure on the air entrainment in the primary breakup zone of high pressure Diesel sprays, Proceedings of ASME Internal combustion Engine Division Fall Technical Conference, ICE-Vol. 39, pp281-288

Soteriou C., Smith M., and Andrews R.(1998) Diesel Injector Laser Light Sheet Illumination of the Development of Cavitation in Orifices, Proc. IMechE C529/018/98

Siebers D.L. (1999) Scaling liquid-phase fuel penetration in Diesel sprays base on mixing-limited vaporization, SAE 1999-01-0528

Wolff M., Delconte A., Schmidt F., Gucher P., and Lemoine F. (2007) High pressure Diesel spray temperature measurements using two-colour laser-induced fluorescence. Meas. Sci. and Technol. 18, pp 697-706